Kelvin-Temperature Ultracold Electron Beam*

Haoyu Huang(黄浩宇)[1,2], Haibo Wang(王海波)[1,2], Jianing Sun(孙佳宁)[1,2], Enliang Wang(王恩亮)[1], Xu Shan(单旭)[1], Chunkai Xu(徐春凯)[1,2**], and Xiangjun Chen(陈向军)[1,2**]

[1]Hefei National Research Center for Physical Sciences at the Microscale and Department of Modern Physics, University of Science and Technology of China, Hefei, Anhui 230026, China
[2]Hefei National Laboratory, University of Science and Technology of China, Hefei, Anhui 230088, China

*Supported by Quantum Science and Technology-National Science and Technology Major Project (Grant No. 2021ZD0303300).
**Corresponding author. Email: xuck@ustc.edu.cn; xjun@ustc.edu.cn

(Received xx August 2026)

We report an ultracold electron beam with Kelvin-level transverse temperature generated from a cold atom electron source by two-color near-threshold photoionization of ^{87}Rb atoms in a magneto-optical trap. A novel self-referenced scheme was employed to precisely determine its transverse temperature. In this scheme, a 3×3 beam array was generated to provide an in situ reference, allowing the transfer-matrix element to be determined directly from the measured grid pattern. The transverse momentum spread of the central beam at the source plane is then retrieved, yielding a transverse temperature of T = 2.0 ± 1.0 K, with the corresponding intrinsic coherence length of L_c = 21.1 ± 5.0 nm and a relative coherence length of $C_\perp$ = (1.3 ± 0.4) × 10^{-3}. The new scheme significantly suppresses the influence of residual magnetic fields, electric field inhomogeneities and electron-optical aberrations. A non-monotonic dependence of the transverse temperature on excess energy was observed and was qualitatively explained by the simulation using a polarization-dependent single-atom Coulomb-Stark trajectory model.

Keywords: cold atom electron source; transverse temperature; coherence length

PACS: 29.25.Bx, 41.75.Fr, 67.85.-d, 42.82.Cr

High-coherence electron beam is essential for electron diffraction and coherent imaging.[1-9] Structural determination of protein microcrystals, in particular, demands a transverse coherence length on the order of tens of nanometers at the specimen.[10] The transverse coherence of the beam is commonly quantified by the relative coherence length $C_\perp = L_c/\sigma_x$, where L_c *is* the transverse coherence length and σ_x is the root-mean-square (rms) beam radius. At the beam waist, L_c can be expressed as $L_c = \hbar/\sigma_{px}$, with σ_{px} denoting the rms transverse momentum spread.[1,2,8,9,11,12] This momentum spread is conventionally parameterized by an effective transverse temperature, $T = \sigma_{px}^2/(m_e k_B)$, leading to $L_c = \hbar/\sqrt{m_e k_B T}$.[3,5,11-14]

In conventional photocathode electron sources, the mean transverse energy is typically ~ 0.5 eV[9] (corresponding to an effective electron temperature ~ 6000 K), having a source coherence length less than 1 nm and a relative coherence length $C_\perp \sim 10^{-4}$. Achieving the required coherence length at the sample therefore necessitates substantial beam expansion,[9,15] which drastically reduces the current density and usable electron flux, rendering single-shot diffraction highly challenging.[16] A more efficient strategy is to increase the coherence length directly at the source. To this end, the Luiten group at the Eindhoven University of Technology proposed a cold atom electron source (CAES) in 2005, predicting source temperature on the order of 10 K.[17]

Following the theoretical proposal, significant experimental advances have been achieved over the past two decades. In 2007, the Luiten group realized the first CAES by combining a magneto-optical trap (MOT) of ^{85}Rb with pulsed-field-ionization of high Rydberg states, yielding an electron beam with 200 ns pulse duration and an effective electron temperature of 500 K.[18] By subsequent optimization of the extraction-electrode geometry, the same group was able to generate electron beams via both photoionization and field-ionization schemes in 2010, reducing the effective transverse temperature to about 10 K.[19] In 2013, utilizing femtosecond-laser ionization and a waist-scan characterization method, they generated picosecond electron bunches with a measured temperature of 18 ± 4 K.[5] The potential of CAES for electron diffraction was demonstrated on a single-crystal graphite film[12] and, more recently, on single-crystal gold using an RF-cavity to accelerate the beam energy from 10 keV to 35 keV.[20] In 2011, the Scholten group at the University of Melbourne demonstrated a CAES based on two-color near-threshold photoionization of ^{85}Rb atoms in MOT.[3,13,14,21-26] By shaping the transverse beam profile into a quasi-uniform distribution using a spatial light modulator (SLM), the source temperature was extracted from the blurring of the sharp edge, yielding a source temperature of $T < 10 \pm 5$ K and a coherence length of $L_c > 10 \pm 3$ nm.[3] They also characterized the coherence length at the source by measuring the visibility of a propagated electron distribution with a sinusoidally modulated profile.[13] Subsequently, a maskless pepper-pot technique was proposed to measure the source emittance and the corresponding coherence length.[14,26] For the μs excitation case, they report a source temperature of $T = 8.4 \pm 0.7$ K and a coherence length of $L_c = 11.8 \pm 1.1$ nm.[26] The Murray group at the University of Manchester implemented an AC-MOT, enabling rapid magnetic-field switching and successfully producing low-energy (~200 eV) electron beam with a transverse temperature of 12.6 ± 0.8 K.[27-30] Furthermore, the Comparat group at the French National Centre for Scientific Research (CNRS) established a Caesium-based CAES[31,32] and most recently, combining a rapid magnetic field switching, a narrow-bandwidth ionization laser, near-threshold photoionization and *s*-polarized ionization laser, they produced electron bunches with a pulse duration of 560 ps.[32]

All the previous studies demonstrated the high coherence of CAES with reported effective transverse temperatures around 10 K, with associated source coherence lengths of about 10 nm. However, simulations by single-atom models of near-threshold photoionization predict that CAES can reach even lower transverse temperature as the excess energy of photoionization approaches zero.[33] The absence of such lower temperatures in previous measurements may arise from two factors. First, the ionization wavelength may not have been tuned sufficiently close to the Stark-shifted ionization threshold, leaving the photoelectrons with some amount of kinetic energy. Second, the measurements may be convolved with contributions from residual magnetic fields, electric field inhomogeneities and electron-optical aberrations, such that the inferred temperature may overestimate the source temperature. Extracting the source temperature from the extrinsic broadening is therefore essential for an accurate assessment of the CAES coherence.

In this letter, we report an ultracold electron beam with Kelvin-level transverse temperature generated from a CAES by two-color near-threshold photoionization of ^{87}Rb atoms in a MOT. A novel self-referenced scheme was proposed to determine the transverse temperature. A 3×3 beam array was generated to provide an in situ reference, allowing the transfer-matrix elements to be determined directly from the measured grid pattern. The transverse momentum spread of the central beam at the source plane is then retrieved. By finely scanning the ionization wavelength around the Stark-shifted threshold using a narrow-linewidth dye laser, lowest transverse temperature of $T = 2.0 \pm 1.0$ K at the source was measured, corresponding to an intrinsic coherence length of $L_c = 21.1 \pm 5.0$ nm and a relative coherence length of $C_\perp = (1.3 \pm 0.4) \times 10^{-3}$. A non-monotonic dependence of the transverse temperature on excess energy was observed and was qualitatively explained by the simulation using a polarization-dependent single-atom Coulomb-Stark trajectory model.

Figure 1 illustrates the experimental configuration and the near-threshold two-color photoionization scheme employed in our ^{87}Rb CAES. Detailed description of the apparatus can be found elsewhere.[34,35]Approximately 10^8 ^{87}Rb atoms were trapped in a MOT at a temperature of ~ 700 μK. A continuous-wave (CW) 780 nm laser, pulsed on for 5 μs, partially excited atoms from

the $5^2S_{1/2}$ ground state to the $5^2P_{3/2}$ state. The spatial intensity profile of this excitation laser was modulated by a SLM (Hamamatsu, X15213-02) to selectively excite the atoms at the designed position within the atom cloud. The excited atoms were subsequently photoionized using a tunable, narrow-linewidth dye laser (~ 480 nm) with a pulse energy of approximately 10 μJ and a pulse duration of approximately 5 ns. By fine-scanning the ionization laser wavelength near the threshold, photoelectrons with near-zero initial kinetic energy were generated, which were then extracted by three ITO-coated electrodes set at -4000 V, 0 V and 0 V. The electrode apertures had a radius of 8 mm, with separations of 50 mm between the first and second electrodes and 10 mm between the second and third electrodes. With the atom cloud positioned midway between the first two electrodes, the ionization region resided at an effective potential of -2000 V, accelerating the electrons to a final kinetic energy of 2 keV at the grounded exit. The resulting electron bunches were detected by a pair of microchannel plates (MCPs) coupled to a phosphor screen (Hamamatsu, F2225-21PGF) and imaged by a CMOS camera (Hamamatsu, ORCA-Flash4.0 V3) 325 mm downstream from the MOT center.

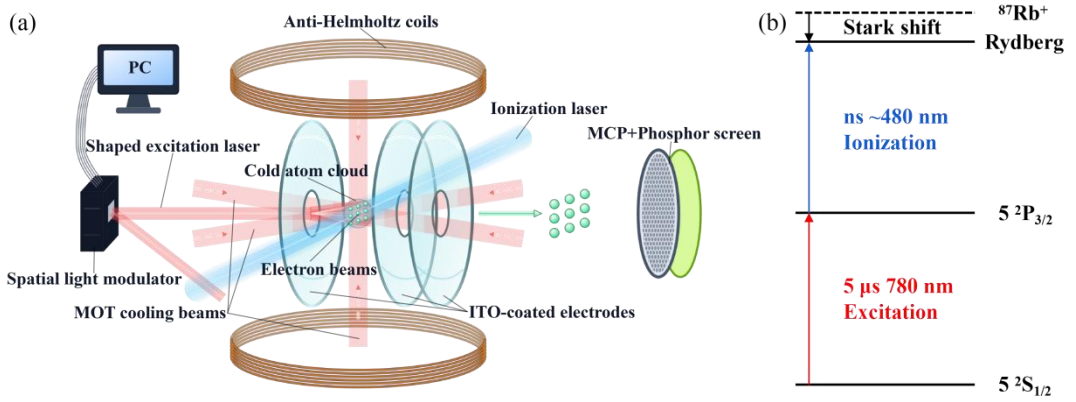

Fig. 1. Experimental scheme and energy-level diagram of the cold atom electron source. (a) Experimental configuration. (b) Energy-level diagram for near-threshold two-color photoionization.

As discussed above, the accurate determination of the source temperature may be compromised by residual magnetic fields, electric field inhomogeneities and electron-optical aberrations. To circumvent these limitations, we introduce a novel self-referenced scheme that deconvolutes such effects, enabling a retrieval of the intrinsic transverse temperature at the source. Adopting electron propagation direction as the *z*-axis and invoking the paraxial approximation, the transverse phase-space coordinates at the detector (x_d, x'_d) are related to those at the source (x_s, x'_s) via the linear transfer matrix:

$$\begin{pmatrix} x_d \\ x'_d \end{pmatrix} = M \begin{pmatrix} x_s \\ x'_s \end{pmatrix} = \begin{pmatrix} M_{11} & M_{12} \\ M_{21} & M_{22} \end{pmatrix} \begin{pmatrix} x_s \\ x'_s \end{pmatrix}. \tag{1}$$

From the first row of Eq. (1), the transverse displacement at the detector is given by $x_d = M_{11}x_s + M_{12}x'_s$. Here, M_{11} represents the transverse magnification, while M_{12} quantifies the mapping from the source divergence angle to the detector-plane displacement. In the present experimental configuration, the electron optical system is well approximated by two drift spaces separated by a single negative lens, as illustrated in Fig. 2(a). Then we have

$$M = M_{d_2} M_f M_{d_1} = \begin{pmatrix} 1 & d_2 \\ 0 & 1 \end{pmatrix} \begin{pmatrix} 1 & 0 \\ -\frac{1}{f} & 1 \end{pmatrix} \begin{pmatrix} 1 & d_1 \\ 0 & 1 \end{pmatrix} = \begin{pmatrix} 1-\frac{d_2}{f} & d_1\left(1-\frac{d_2}{f}\right)+d_2 \\ -\frac{1}{f} & 1-\frac{d_1}{f} \end{pmatrix}, \tag{2}$$

where f is the focal length of the negative lens, and d_1, d_2 denote the drift lengths before and after the lens, respectively. The transfer matrix element M_{12} is therefore given by $M_{12} = d_1M_{11} + d_2$.

At the source plane, the transverse position and divergence angle are uncorrelated. Consequently, the rms beam size at detector plane is

$$\sigma_{x_d} = \sqrt{M_{11}^{\ 2}\sigma_{x_s}^2 + M_{12}^{\ 2}\sigma_{x_s'}^2}\,, \tag{3}$$

where σ_{x_s} and σ_{x_d} are the rms beam sizes at the source and detector planes, respectively, and $\sigma_{x_s'}$ is the angular spread at the source. Therefore, once M_{11}, σ_{x_d} and σ_{x_s} are known, the source angular spread is obtained as

$$\sigma_{x_s'} = \frac{\sqrt{\sigma_{x_d}^2 - M_{11}^2\sigma_{x_s}^2}}{d_1 M_{11} + d_2}. \tag{4}$$

The effective transverse temperature is then given by [14]

$$T = \frac{\sigma_{p_x}^2}{m_e k_B} = \frac{2U\sigma_{x_s'}^2}{k_B}, \tag{5}$$

where U is the electron kinetic energy, m_e is the electron mass, and k_B is the Boltzmann constant. The transverse momentum spread $\sigma_{p_x} = \sqrt{2m_e U}\,\sigma_{x_s'}$.

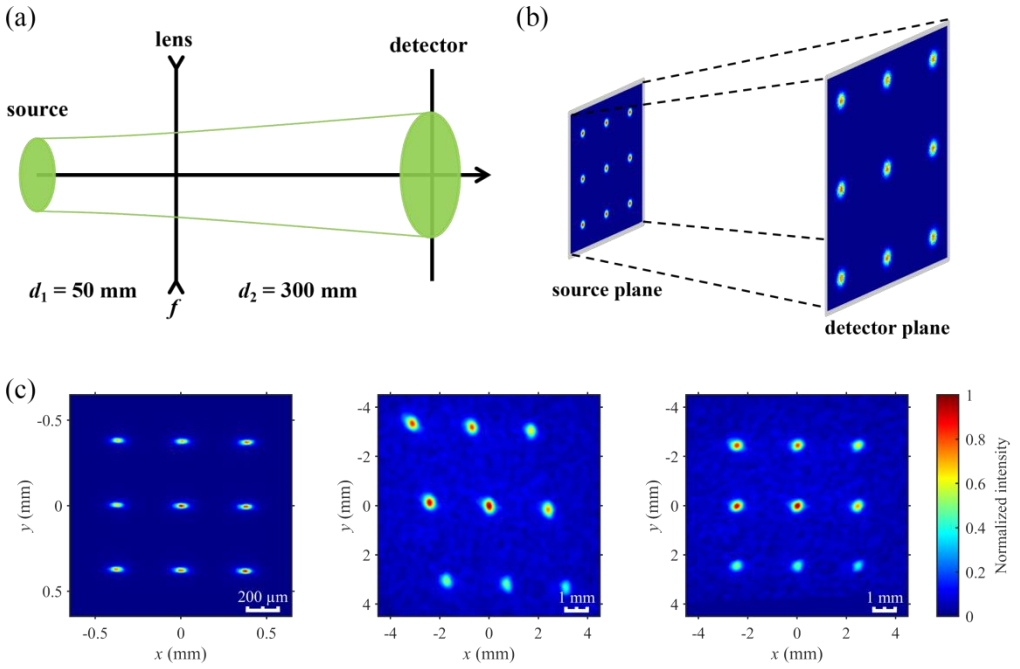

Fig. 2. (a) Equivalent electron-optical system. (b) Simulation of the source-to-detector transportation by General Particle Tracer [36] package. (c) Electron-beam profiles at the source plane (left), at the detector (middle), and after distortion-correction (right).

To determine the transfer-matrix element M_{11} (i.e. the transverse magnification), the spatial intensity profile of the excitation laser was modulated by the SLM into a 3×3 grid, generating a corresponding electron beam array (3×3 with 560 μm spacing) for referencing. This beam array was extracted, accelerated and transported to the detector. Ideally, M_{11} can be given by the geometric magnification of the grid pattern. However, the experimentally recorded pattern on the detector (middle panel of Fig. 2(c)) exhibits significant distortions due to residual magnetic fields, electric field inhomogeneities and electron-optical aberrations. This precludes a reliable extraction of M_{11} via simple geometric scaling.

To address this, we employed General Particle Tracer [36] package to simulate the transportation of the 3×3 source beam array to the detector under the experimental condition, as depicted in Fig. 2(b). The electron source was modeled as a 3×3 array in x-y plane. Each beamlet has a 2D Gaussian spatial distribution with a standard deviation of 30 μm, and the spacing between adjacent beamlets

is 560 μm. We therefore obtained a simulated non-distorted pattern at the detector plane. By reading the coordinates of the beams in both the simulated and the measured beam arrays at the detector, mapping between them can be established through a projective transformation matrix. This transformation matrix was then used to correct the measured pattern at the detector plane. The resulting distortion-corrected beam array is shown in the right panel of Fig. 2(c), from which $M_{11} \approx$ 4.4 was extracted.

With M_{11} determined, the transverse temperature of the central beam was evaluated using Eqs. (4) and (5). At the source, the spatial profile of the electron beam was approximated by the SLM-imprinted intensity distribution of the excitation laser, which was measured using a beam profiler (Ophir, SP932U). This is reasonable because, under the present non-saturated conditions (~ 1 μW of the excitation laser power), the spatial distribution of atoms in excited state is identical to the optical distribution and subsequent ionization of the excited atoms yields an identical electron distribution. As shown in the left panel of Fig. 2(c), the central beam exhibited obvious asymmetry. This asymmetry arises from asymmetric focusing (astigmatism) in the *x* and *y* directions, caused by the slightly oblique incidence of the excitation laser beam on the reflective SLM. We employed a two-dimensional Gaussian function to fit the beam profile, which yielded rms beam size of σ_{x_s} = 30 ± 4 μm and σ_{y_s} = 9 ± 4 μm. At the detector plane, the distortion-corrected beam (right panel of Fig. 2(c)) also displayed asymmetry. Fitting the corrected beam profile with a two-dimensional Gaussian function provided the rms beam size at the detector. The detector resolution 48 ± 3.4 μm (evaluated by the point-spread function through measuring the averaged spatial distributions of the images over 100 single electrons) should be deconvoluted from the fitting results, giving σ_{x_d} and σ_{y_d}. This asymmetry does not influence the extracted transverse temperature since the source angular spread is independent of the source size. Therefore, we employed the geometric mean of the source angular spreads derived from both *x* and *y* dimensions to extract the effective source transverse temperature according to Eqs. (4) and (5), from which the coherence length can be calculated.

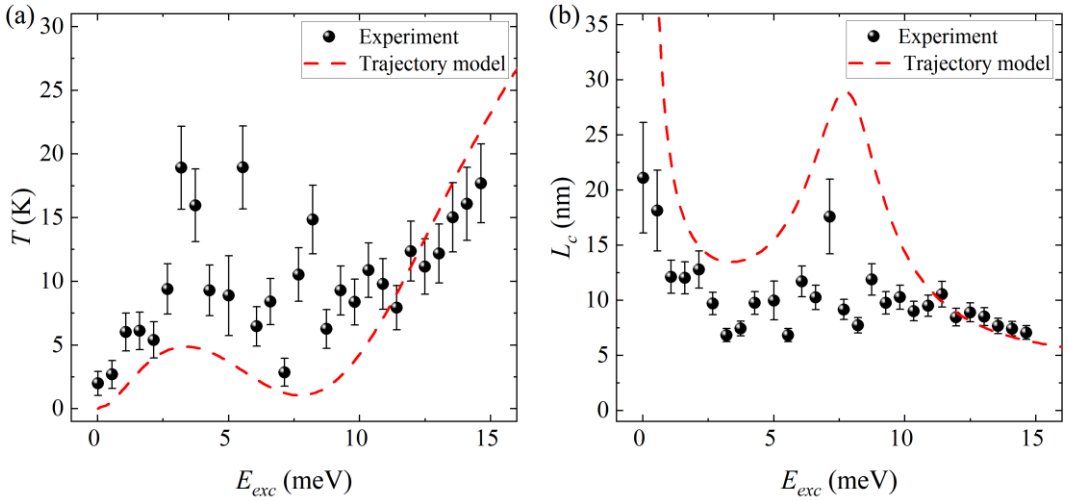

Fig. 3. Source transverse temperature and coherence length as functions of excess energy.

In our experiment, the ionization laser wavelength was finely scanned to reduce the excess energy of photoionization to meV regime. It should be noted that the applied extraction field (0.08 MV/m) induces a Stark shift, lowering the ionization threshold to approximately 483 nm. We systematically measured the effective transverse temperature *T* and coherence length L_c at the source as a function of excess energy E_{exc} over the Stark-shifted ionization threshold. The results are shown in Fig. 3. The measured transverse temperature shows non-monotonic dependence on excess energy

with minima at threshold and at ~7.8 meV. To our best knowledge, this is the first experimental observation of a minimum in the transverse temperature at a finite excess energy. This behavior can be qualitatively reproduced by the simulation (dashed red lines in Fig. 3, see Supplementary Material for details) employing a polarization-dependent single-atom Coulomb-Stark trajectory model.[33,37] Physically, the Coulomb potential of the residual ion and the static extraction field form a bottleneck near the saddle-point, acting as a focusing lens. At specific excess energies, namely at threshold and at ~7.8 meV, this lens collimates the photoelectrons into a nearly parallel beam, thereby minimizing the transverse momentum spread. At the ionization threshold, corresponding to wavelength of 483.1383 nm, the rms beam size at the detector plane was measured to be σ_{x_d} = 169.4 ± 2.2 μm and σ_{y_d} = 111.1 ± 1.6 μm. The source transverse temperature was then extracted to be T = 2.0 ± 1.0 K, corresponding to an intrinsic coherence length L_c = 21.1 ± 5.0 nm and a relative coherence length $C_\perp = (1.3 \pm 0.4) \times 10^{-3}$. We note that space charge effect can broaden the beam and lead to an overestimation of the source temperature. However, under our experimental conditions, the number of electrons per pulse was estimated to be on the order of several tens, corresponding to a bunch charge of approximately 0.01 fC. GPT simulations incorporating space-charge effects for a 100-electron pulse with a 30 μm rms size yield an rms beam size of 299 ± 4 μm at the detector-plane, while simulations without space charge effects give 300 μm. The results indicate that space-charge-induced broadening is negligible in the low-charge, nanosecond-bunch regime used here, consistent with previous work.[14]

In summary, we generated an ultracold electron beam with a Kelvin-scale transverse temperature from a cold atom electron source, utilizing two-color near-threshold photoionization of ^{87}Rb atoms confined in a magneto-optical trap. By employing a novel self-referenced scheme that suppresses the influence of residual magnetic fields, electric field inhomogeneities and electron-optical aberrations, the transverse temperature of the electron beam was precisely determined. In the scheme, by modulating the spatial intensity profile of the excitation laser using SLM, a 3×3 electron beam array was generated to provide an in situ reference. From the measured grid pattern of the distortion-corrected beam array, the transfer-matrix element M_{11} (i.e. the transverse magnification) was determined. Further measuring the rms beam sizes at the source and at the detector, we obtained the transverse momentum spread of the central beam. Consequently, the transverse temperature was deduced. By finely scanning the ionization wavelength around the Stark-shifted threshold using a narrow-linewidth dye laser, the lowest transverse temperature of T = 2.0 ± 1.0 K at the source was measured, corresponding to an intrinsic coherence length of L_c = 21.1 ± 5.0 nm and a relative coherence length of $C_\perp = (1.3 \pm 0.4) \times 10^{-3}$, representing a substantial improvement over the previous CAES studies, which reported transverse temperatures of approximately 10 K and source coherence lengths of approximately 10 nm. Meanwhile, a non-monotonic dependence of the transverse temperature on excess energy was observed and was qualitatively explained by the simulation using a polarization-dependent single-atom Coulomb-Stark trajectory model. This significant enhancement in source coherence directly increases the reduced brightness at given bunch charge, which is a critical figure of merit for electron sources. Recent simulation study points out that an optical lattice could suppress the disorder-induced heating,[38] potentially enabling higher bunch charges while keeping coherence high, and therefore may pave the way for high-resolution, single-shot diffraction and imaging experiments. On the other hand, the picosecond pulse duration[14] of CAES sources makes it possible to perform time-resolved experiments in the future.

References

[1] van Oudheusden T, Pasmans P L E M, van der Geer S B, de Loos M J, van der Wiel M J, and Luiten O J 2010 *Phys. Rev. Lett.* **105** 264801

[2] Sciaini G and Miller R J D 2011 *Rep. Prog. Phys.* **74** 096101

[3] McCulloch A J, Sheludko D V, Saliba S D, Bell S C, Junker M, Nugent K A, and Scholten R E 2011 *Nat. Phys.* **7** 785

[4] Paarmann A, Gulde M, Müller M, Schäfer S, Schweda S, Maiti M, Xu C, Hohage T, Schenk F, Ropers C, and Ernstorfer R 2012 *J. Appl. Phys.* **112** 113109

[5] Engelen W J, van der Heijden M A, Bakker D J, Vredenbregt E J D, and Luiten O J 2013 *Nat. Commun.* **4** 1693

[6] Hoffrogge J, Stein J P, Krüger M, Förster M, Hammer J, Ehberger D, Baum P, and Hommelhoff P 2014 *J. Appl. Phys.* **115** 094506

[7] Ehberger D, Hammer J, Eisele M, Krüger M, Noe J, Högele A, and Hommelhoff P 2015 *Phys. Rev. Lett.* **114** 227601

[8] Feist A, Bach N, da Silva N R, Danz T, Moeller M, Priebe K E, Domroese T, Gatzmann J G, Rost S, Schauss J, Strauch S, Bormann R, Sivis M, Schaefer S, and Ropers C 2017 *Ultramicroscopy* **176** 63

[9] Filippetto D, Musumeci P, Li R K, Siwick B J, Otto M R, Centurion M, and Nunes J P F 2022 *Rev. Mod. Phys.* **94** 045004

[10] Kirchner F O, Lahme S, Krausz F, and Baum P 2013 *New J. Phys.* **15** 063021

[11] Engelen W J, Smakman E P, Bakker D J, Luiten O J, and Vredenbregt E J D 2014 *Ultramicroscopy* **136** 73

[12] van Mourik M W, Engelen W J, Vredenbregt E J D, and Luiten O J 2014 *Struct. Dyn.* **1** 034302

[13] Saliba S D, Putkunz C T, Sheludko D V, McCulloch A J, Nugent K A, and Scholten R E 2012 *Opt. Express* **20** 3967

[14] McCulloch A J, Sheludko D V, Junker M, and Scholten R E 2013 *Nat. Commun.* **4** 1692

[15] Zernike F 1938 *Physica* **5** 785

[16] Speirs R W, Putkunz C T, McCulloch A J, Nugent K A, Sparkes B M, and Scholten R E 2015 *J. Phys. B: At. Mol. Opt. Phys.* **48** 214002

[17] Claessens B J, van der Geer S B, Taban G, Vredenbregt E J D, and Luiten O J 2005 *Phys. Rev. Lett.* **95** 164801

[18] Claessens B J, Reijnders M P, Taban G, Luiten O J, and Vredenbregt E J D 2007 *Phys. Plasmas* **14** 093101

[19] Taban G, Reijnders M P, Fleskens B, van der Geer S B, Luiten O J, and Vredenbregt E J D 2010 *Europhys. Lett.* **91** 46004

[20] Nijhof D F J, de Raadt T C H, Huijts J, Franssen J G H, Mutsaers P H A, and Luiten O J 2023 *Struct. Dyn.* **10** 054303

[21] McCulloch A J, Sparkes B M, and Scholten R E 2016 *J. Phys. B: At. Mol. Opt. Phys.* **49** 164004

[22] Thompson D J, Murphy D, Speirs R W, van Bijnen R M W, McCulloch A J, Scholten R E, and Sparkes B M 2016 *Phys. Rev. Lett.* **117** 193202

[23] McCulloch A J, Speirs R W, Grimmel J, Sparkes B M, Comparat D, and Scholten R E 2017 *Phys. Rev. A* **95** 063845

[24] Speirs R W, McCulloch A J, Sparkes B M, and Scholten R E 2017 *Phys. Rev. A* **95** 053408

[25] Torrance J S, Speirs R W, McCulloch A J, and Scholten R E 2018 *Phys. Rev. Accel. Beams* **21** 032802

[26] McCulloch A J 2013 *Generation of shaped cold electron bunches for ultrafast electron diffraction* (Ph.D. dissertation) (Melbourne: University of Melbourne)

[27] Harvey M and Murray A J 2008 *Phys. Rev. Lett.* **101** 173201

[28] Xia G, Harvey M, Murray A J, Bellan L, Bertsche W, Appleby R B, Mete O, and Chattopadhyay S 2014 *J. Inst.* **9** P06011

[29] Jones M, Harvey M, Bertsche W, Xia G, Chattopadhyay S, Murray A J, and Appleby R 2017 *J. Phys.: Conf. Ser.* **875** 052020

[30] Jones M 2019 *The AC-MOT Cold Atom Electron Source* (Ph.D. dissertation) (Manchester: University of Manchester)

[31] Fedchenko O, Chernov S, McCulloch A, Vielle-Grosjean M, Comparat D, and Schönhense G 2017 *Appl. Phys. Lett.* **111** 021104

[32] Fedchenko O, Chernov S, Schönhense G, Hahn R, and Comparat D 2020 *Phys. Rev. A* **101** 013424

[33] Engelen W J, Vredenbregt E J D, and Luiten O J 2014 *Ultramicroscopy* **147** 61

[34] Wang H B, Huang H Y, Sun J N, Xu C K, Wang E L, Shan X, and Chen X J 2026 *J. Appl. Phys.* **139** 194902

[35] Wang H B, Huang H Y, Sun J N, Xu C K, Wang E L, Shan X, and Chen X J 2026 *Chin. Phys. B* https://iopscience.iop.org/article/10.1088/1674-1056/ae64d2

[36] Pulsar Physics *General Particle Tracer* https://www.pulsar.nl/gpt/

[37] Engelen W J, Bakker D J, Luiten O J, and Vredenbregt E J D 2013 *New J. Phys.* **15** 123015

[38] Wang H B, Yao Z L, Huang H Y, Sun J N, Zhou F Y, Wu Y, Wang J G, and Chen X J 2024 *Phys. Plasmas* **31** 052114